Reprint from

Glastechnische Berichte

International Journal of Glass Science and Technology

Vol. 63 (1990)

Verlag der Deutschen Glastechnischen Gesellschaft
Frankfurt am Main

Original Paper

Thermal comparison of glass furnace operation with oil and natural gas

Maria da Graça Carvalho
Instituto Superior Técnico, Mechanical Engineering Department, Lisbon (Portugal)

Frederik C. Lockwood
Imperial College of Science, Technology and Medicine, Mechanical Engineering Department, London (Great Britain)

Natural gas and fuel oil firing are compared for an industrial glass furnace by means of a three-dimensional computer simulation comprising sub-models for turbulence, combustion and thermal radiation. The heat transfer by thermal radiation from the flame and the furnace structure to the glass bath is discussed for both fuels. The total radiative heat flux to the glass is found to be 5 % higher for the case of the oil-fired furnace, while the distribution of heat flux to the glass was found to be less uniform. The heat flux intensities to the glass near the burner are much greater with oil flames because of their greater flame emissivities. But in the regions where combustion is complete heat transfer to the glass from the combustion gases is found to be more intense for natural gas. Comments are made on furnace ageing and pollution emission.

Thermischer Vergleich zwischen ölbeheizten und erdgasbeheizten Glasschmelzöfen

Mit Hilfe einer dreidimensionalen Computersimulation, die Unterprogramme für Turbulenz-, Verbrennungs- und Wärmestrahlungsberechnungen umfaßt, wird für einen Glasschmelzofen die Erdgas- mit einer Ölbeheizung verglichen. Der Wärmeübergang durch thermische Strahlung von der Flamme und den Ofenteilen zum Glasbad wird für beide Brennstoffe diskutiert. Der Gesamtstrahlungswärmefluß ist für den Fall des ölbeheizten Ofens um 5 % höher; dagegen wurde eine ungleichmäßigere Verteilung des Wärmeflusses zum Glas festgestellt. Infolge ihrer höheren Emissionen ist in der Nähe des Brenners die Wärmestromintensität von Ölflammen sehr viel größer. Jedoch wurde in den Bereichen vollständiger Verbrennung für Erdgas als Brennstoff ein sehr viel intensiverer Wärmeübergang von den Verbrennungsgasen zum Glas festgestellt. Kommentare zur Ofenalterung und zur Emission von Verunreinigungen werden gegeben.

1. Introduction

With the discovery and subsequent distribution of large quantities of natural gas, many conversions from oil to gas firing of industrial appliances as well as the construction of new gas-fired plants are either taking place or being contemplated.

The present paper presents a comparison between oil and natural gas for the particular case of an end-port regenerative industrial glass furnace. In a glass melting furnace, the glass batch receives heat predominantly by radiation from the flames and the incandescent refractory surfaces. Convection from the flow constitutes a relatively minor portion of the total heat transfer. In the present work the different characteristics of heat transfer from oil and natural gas flames particularly with regard to the nature of the thermal radiation emissions from the two types of flames are investigated.

A proper comparison between the performance of natural gas and oil flames necessitates an accurate calculation of the radiative heat transfer characteristics of the flame. However, most of the published works on the comparison of natural gas and oil firing are based on experimental techniques or overall enthalpy balances. In an early study, Wu [1] compared experimentally the performance of natural gas flames and oil flames for a cylindrical water-cooled furnace. In this case the measurements showed that the overall efficiency remained approximately the same when natural gas was substituted for oil as the natural gas flame contributes to better convective heat transfer to the cooled parts of the furnace, and it is also somewhat hotter. Since then, there have been many studies mostly in experimental furnaces. The most important contributions have originated from groups at the International Flame Research Foundation (IFRF (e.g. [2])) and in the Groupe d'Etude des Flammes de Gaz Naturel (GEFGN (e.g. [3])).

Pai et al. [2] investigated the influence of operational variables (fuel type, load, burner type, excess air, preheat and oxygen enrichment of combustion air) on the heat transfer to a calorimetric hearth in the IFRF furnace. The fuels investigated were natural gas, blast furnace gas, blast furnace gas-natural gas mixtures and heavy fuel oil. The experimental data were used to test and develop a three-dimensional prediction procedure. Conclusions about the influence of each operational variable were drawn. Regarding the fuel type, their findings showed that the change from natural gas to heavy fuel oil (at constant thermal input and excess air factor) resulted in an increase in efficiency of about 10 %, but changes in local heat fluxes were much greater, up to some 25 % in the peak heat flux.

Received 5 February 1990.

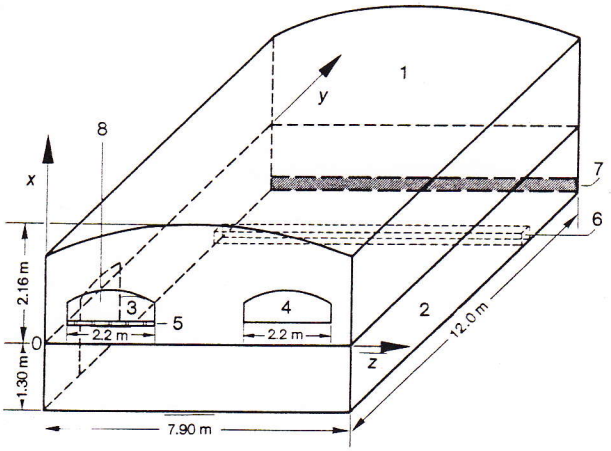

Figure 1. Sketch of an end-port regenerative glass melting furnace. 1: combustion chamber, 2: glass melt container, 3: inlet port, 4: outlet port, 5: five fuel injectors, 6: step, 7: throat, 8: feed of frit and cullet.

The purpose of work of the GEFGN was to promote the industrial utilization of natural gas by means of systematic tests carried out mainly on an experimental furnace in Toulouse (France). Tests with natural gas, fuel oil, and mixtures of the two have been performed [3]. The GEFGN derived a formulation for the dimension of burners in accordance with the demanded flame characteristics. A formulation giving the optimal dosage of the two fuels (natural gas and fuel oil) for a global fuel economy was also recommended. Some work has been done in this field applied to glass furnaces, but most of it is based on measurements and visual observations of furnace performance backed-up by a small amount of theory. The thermal efficiency of an American oil-fired furnace was compared with that of the same furnace burning natural gas [4]. The semi-luminous natural gas firing in that case was 4 % more thermally efficient than heavy oil firing. Short-term European production trials with natural gas have been less favourable. Buschmann [5] in Germany reported a 5 % increase in energy consumption over fuel oil, and de Lange [6] in Holland an 8 % increase. These results are strongly correlated with the composition of the natural gas used. The American fuel contains 0.5 % nitrogen, whereas the German and Dutch fuels contain 2.5 and 14.5 % nitrogen, respectively. Leveque [7] compared the performance of a cross-fired glass furnace working with natural gas and heavy fuel oil. His study was based on an overall enthalpy balance of the furnace. The results were only valid for cross-fired furnaces in which the length and development of the flame were limited by a somewhat restricted furnace width. He concluded that for high-temperature glass melting furnaces the fuel consumption is some 7 % more for the natural gas than for the heavy oil firing.

A comparison between oil and natural gas fuels as applied mainly to cross-fired regenerative glass furnaces was discussed by Abbott [8]. He concludes that melting rates, achieved with natural gas firing are as good as those attained on oil and that in general natural gas fired furnaces will have longer lives.

In the present paper the comparison of the performance of an industrial glass furnace firing gas or fuel oil is made by means of a three-dimensional computer simulation comprising sub-models for turbulence, combustion and thermal radiation. It is believed that it is the first time that such a comparison for industrial conditions based on the application of a three-dimensional computer code has been reported in the literature.

2. Description of the furnace

Figure 1 shows a sketch of the furnace which is of the end-port regenerative type. The fuel is admitted from five burners situated in a port which admits preheated air. The flame forms a loop within the combustion chamber and exits through the partner port. This port also contains a burner row and the furnace is alternatively fired from each port to enhance the uniformity of heat transfer to the glass surface. Since the time between port switching is relatively long the consequential transient effects are ignored and steady-state calculations are performed.

The air flow is directed downwards at an angle of 16° while the fuel jets have an adjustable upward inclination, the usual value being 8°. The furnace crown and side walls are refractory-lined and the crown is arched as indicated in figure 1. The batch, which is a mixture of sand (frit) and recycled glass (cullet) enters via the port. The molten glass exits from the throat.

3. Physical modelling

The governing transport equations for the mean motion of a turbulent three-dimensional flow were applied in their curvilinear orthogonal co-ordinate form.

3.1. Mean flow equations

The time-averaged equations for the conservation of momentum may, in compact tensor notation, be expressed as:

$$\frac{\partial}{\partial x_j}\left(\overline{\varrho\, u_j u_i} + \overline{p\,\delta_{ij}} - \mu\left[\frac{\overline{\partial u_i}}{\partial x_j} + \frac{\overline{\partial u_j}}{\partial x_i} - \frac{2}{3}\frac{\overline{\partial u_k}}{\partial x_k}\overline{\delta_{ij}}\right]\right) -$$

$$-(\overline{\varrho} - \overline{\varrho}_{\mathrm{ref}})\, g_i + \frac{\partial}{\partial x_j}\,\overline{\varrho\, u_j' u_i'} = 0\,. \qquad (1)$$

Here u_i is the velocity in the direction of the coordinate x_i, $\overline{\varrho}$ is the density and $\overline{\varrho}_{\mathrm{ref}}$ a reference

value, g_i is the magnitude of the gravitational acceleration in the i direction, p is the pressure, μ is the laminar viscosity, and the operator δ_{ij} is the unity for $i = j$ and zero when $i \neq j$.

The equations for the conservation of a chemical species, l, and of energy may be respectively expressed as:

$$\frac{\partial}{\partial x_i}(\overline{\varrho\, u_i}\,\overline{m_l}) - \frac{\partial}{\partial x_i}\left(\Gamma_l \frac{\partial \overline{m_l}}{\partial x_i} - \overline{\varrho\, u_i' m_l'}\right) - \overline{P_l} = 0 \quad (2)$$

and

$$\frac{\partial}{\partial x_i}(\overline{\varrho\, u_i}\,\overline{\tilde{h}}) - \frac{\partial}{\partial x_i}\left(\Gamma_h \frac{\partial \overline{\tilde{h}}}{\partial x_i}\right) + \frac{\partial}{\partial x_i}\overline{\varrho\, u_i'' \tilde{h}''} - \overline{S} = 0\,. \quad (3)$$

In equation (2) m_l stands for the mass fraction of l, Γ_l is the mass diffusion coefficient for this species, and P_l is its chemical rate of production. In equation (3), $\tilde{h}$ represents the stagnation enthalpy, Γ_h is equal to the fluid thermal conductivity divided by its constant-pressure specific heat, and $\overline{S}$ is a source term defined by:

$$\overline{S} = \overline{Q}_{\mathrm{rad}} \quad (4)$$

where $\overline{Q}_{\mathrm{rad}}$ is the net volumetric heat gain due to thermal radiation.

In addition to equations (2 to 4) the equation of mass continuity

$$\frac{\partial}{\partial x_i}(\overline{\varrho\, u_i}) = 0 \quad (5)$$

must be included.

3.2. Turbulence model

The "two-equation" model [9], in which equations for the kinetic energy of turbulence, k, and its dissipation rate, ε, are solved, is considered appropriate. The correlations in equation (1) are expressed, in analogy with laminar flow [10], as:

$$-\overline{\varrho\, u_j' u_i'} = \mu_t\left(\frac{\partial \overline{u_i}}{\partial x_j} + \frac{\partial \overline{u_j}}{\partial x_i} - \frac{2}{3}\frac{\partial \overline{u_k}}{\partial x_k}\delta_{ij}\right) \quad (6)$$

where μ_t is a turbulent viscosity that may be related to k and ε by dimensional arguments:

$$\mu_t = C_\mu\, \overline{\varrho}\, k^2 / \varepsilon \quad (7)$$

where C_μ is a constant of the model. The turbulent exchange coefficient $\Gamma_{\phi,t}$ for any variable ϕ (where ϕ stands for a surrogate variable representing f, g, $\tilde{h}$, k, m_s, and ε), may be expressed as:

$$\Gamma_{\phi,t} = \mu_t / \sigma_{\phi,t} \quad (8)$$

where $\sigma_{\phi,t}$ is a turbulent Prandtl number of order unity. Turbulent transport correlations involving ϕ' are determined from the Boussinesq approximation:

$$\overline{\varrho\, u_i' \phi'} = \Gamma_{\phi,t}\,\overline{\partial\phi / \partial x_i}\,. \quad (9)$$

The following differential equations for k and ε to be solved are:

$$\frac{\partial}{\partial x_j}(\overline{\varrho\, u_j}\, k) - \frac{\partial}{\partial x_j}\left(\Gamma_k \frac{\partial k}{\partial x_j}\right) - \\ - \mu_t \frac{\partial \overline{u_i}}{\partial x_j}\left(\frac{\partial \overline{u_i}}{\partial x_j} + \frac{\partial \overline{u_j}}{\partial x_i}\right) + C_D\, \overline{\varrho}\, \varepsilon = 0 \quad (10)$$

and

$$\frac{\partial}{\partial x_j}(\overline{\varrho\, u_j}\, \varepsilon) - \frac{\partial}{\partial x_j}\left(\Gamma_\varepsilon \frac{\partial \varepsilon}{\partial x_j}\right) - \\ - C_1 \mu_t \frac{\varepsilon}{k}\frac{\partial \overline{u_i}}{\partial x_j}\left(\frac{\partial \overline{u_i}}{\partial x_j} + \frac{\partial \overline{u_j}}{\partial x_i}\right) + C_2\, \overline{\varrho}\, \frac{\varepsilon^2}{k} = 0 \quad (11)$$

where C_1, C_2 and C_D are further constants and Γ_k and Γ_ε are determined via equation (8).

The model constants presently used are those established in many previous furnace applications (e.g. [11]).

3.3. Combustion model

The combustion model is based on the ideal of a single-step and fast chemical reaction between the gaseous fuel and oxidant, assumed to combine in stoichiometric proportions. Equal effective turbulent mass diffusion coefficients for the fuel and oxidant and an instantaneous reaction are also assumed [12]. As a consequence of these assumptions the flame thermodynamic state becomes related to a single passive scalar:

$$\Phi \equiv s_{\mathrm{ox}}\, m_{\mathrm{fu}} - m_{\mathrm{ox}} \quad (12)$$

where s_{ox} is the stoichiometric oxygen requirement by mass and m_{fu} and m_{ox} are the fuel and oxidant mass fractions.

The mixture fraction f is related to this quantity by:

$$f \equiv (\Phi - \Phi_0) / (\Phi_1 - \Phi_0) \quad (13)$$

where the subscripts 1 and 0 designate the fuel- and oxidant-bearing streams. The assumption that the chemical kinetic rate is fast (with respect to the turbulent transport rate) implies that fuel and oxidant

cannot coexist, so $m_{fu} = 0$ for $m_{ox} \geqq 0$ and $m_{ox} = 0$ for $m_{fu} \geqq 0$, and the concentrations m_{fu} and m_{ox} are related linearly to f through equations (12 and 13).

The transport equation for the mixture fraction is given by:

$$\frac{\partial}{\partial x_i}(\overline{\varrho u_i} f) - \frac{\partial}{\partial x_i}\left(\Gamma_f \frac{\partial f}{\partial x_i}\right) = 0. \tag{14}$$

It may be noted that the above modelling presumes a stationary thin flame envelope. The fluctuating nature of the turbulent reaction can be accommodated through a modelled equation for the variance of the mixture-fraction fluctuations.

A statistical approach is used to describe the temporal nature of the mixture-fraction fluctuations. The time-averaged value of any property ϕ, solely dependent on f, can then be determined from:

$$\phi = \int_0^1 \varphi(f)\, P(f)\, \mathrm{d}f. \tag{15}$$

In the present work, the "clipped normal" probability density function [13] which is characterised by just two parameters, and the mean square of the fluctuations $g \equiv \overline{(f - \bar{f})^2}$, is assumed. A modelled transport equation has been derived [14] for g which runs:

$$g = \frac{\partial}{\partial x_i}(\overline{\varrho u_i} g) - \frac{\partial}{\partial x_i}\left(\Gamma_g \frac{\partial g}{\partial x_i}\right) - \\ - C_{g1}\, \mu_t \left(\frac{\partial f}{\partial x_i} \cdot \frac{\partial f}{\partial x_i}\right) - \frac{C_{g2}}{k} \bar{\varrho}\, \varepsilon\, g = 0 \tag{16}$$

where C_{g1} and C_{g2} are additional adjustable parameters.

A simple and economical model for oil-fired furnaces is used in which it is assumed that the oil spray evaporates instantaneously. This is justified in glass furnaces where the droplet vaporisation times are very short compared to the flame residence times.

3.4. Thermodynamics model

The mixture specific enthalpy may be defined by:

$$\bar{h} \equiv \int_0^T \sum_j \overline{m}_j\, C_{pj}(T)\, \mathrm{d}T + \overline{m}_{fu}\, H \tag{17}$$

where C_{pj} is the constant-pressure specific heat of a species j.

Density is determined from the equation of state,

$$\bar{\varrho} = p\, (R\, \bar{T} \sum_j \overline{m}_j / M_j)^{-1} \tag{18}$$

where R is the universal gas constant, and M_j is the molecular weight of species j. Since the values of m_j, as well as T, are all functions of f, the time-averaged density for use in the mean flow equations is again determined from equation (15).

3.5. Soot model

The distinctive feature of oil-fired flames is their significant soot content. The proportion of the total carbon content of the fuel which converts to soot is too small to influence significantly the overall flame heat release distribution. Rather, soot is of concern because its presence greatly augments the radiation heat transfer and because it is a pollutant. Most reasonably operated and maintained modern burners ensure complete combustion of soot. So the primary function of the soot model will be the good characterising of the optical behaviour of the flame. The soot content of heavy-oil flames is so large that those of industrial dimensions approach the black body limit. In consequence the accurate prediction of the local soot concentration is not a prerequisite for the good calculation of the radiation transfer. This is indeed fortunate since the mechanisms of soot formation are far from being established even in the simplest laboratory flames [15].

A simple global expression similar to that used by Khan and Greeves [16] is chosen to characterise soot production:

$$P_{s+} = C_f\, P_{fu}\, \Phi^n \exp(-E\, R / T_g). \tag{19}$$

C_f is a function which ideally depends on an easily definable fuel property such as the C / H ratio. Although the work of Khan and Greeves was performed in connection with Diesel engines it was found that their values of $n = 3$ and the activation energy $E = 168\,438$ J/mol are useful. However, for C_f the value tuned by Abbas and co-workers [17] for the case of furnaces was found appropriate. Soot production is essentially zero for equivalence ratios, Φ, less than that corresponding to the incipient sooting limit [18] and for Φ in excess of a value corresponding roughly to the upper flammability limit. Following Khan and Greeves the upper and lower limits of Φ have been set to 2 and 8, respectively.

To an extent the determination of the soot-burning rate poses a less demanding modelling problem since the particle sizes are so small that near-particle diffusion cannot possibly be controlled, rather the combustion rate will be controlled by the rate of mixing of the particle-bearing vortices with adjacent oxygen-bearing material. A straightforward method of estimating this rate has been proposed by Magnussen and Hjertager [19], who, following conventional turbulence concepts [20], presume that the mixing rate is proportional to the magnitude of the local time mean soot concentration, and the time

scale of the large scale turbulence motion ε / k. Their expression for the soot consumption rate is:

$$P_{s-} = A\,\overline{m}_s\,(\varepsilon / k) \tag{20}$$

where A is a model constant assigned the value 4 based on numerical experimentation. This relation will not be satisfactory in regions where the reaction rate is limited by oxygen deficiency in which case Magnussen and Hjertager [19] propose:

$$P_{s-} = A\left(\frac{\overline{m}_{ox}}{\overline{m}_s\,\bar{s}_s + \overline{m}_{fu}\,\bar{s}_{fu}}\right)\overline{m}_s\left(\frac{\varepsilon}{k}\right) \tag{21}$$

where $\bar{s}_s$ and $\bar{s}_{fu}$ are the soot and fuel stoichiometric ratios. The alternative giving the smallest reaction rate is to be used.

3.6. Radiation model

The "discrete transfer" radiation prediction procedure of Lockwood and Shah [21] has been utilised in this study. This method combines ease of use, economy and flexibility of application. This last feature is of particular importance in the real world of geometrically intricate combustion chambers. The claimed advantages of the method have now survived the rigours of a great many industrial applications (e.g. [22 and 23]).

The "discrete transfer" method is founded on a direct solution of the radiation-transfer equation for a direction which runs:

$$\frac{\mathrm{d}I}{\mathrm{d}l} = (k_g + k_s)\left(\frac{\tilde{E}}{\pi} - I\right) \tag{22}$$

where I is the radiation intensity in a selected direction, l is the distance in that direction, $\tilde{E}(T) \equiv \sigma\,T_g^4$ is the black body emissive power, and k_g and k_s are the gas and soot absorption coefficients, respectively. The scattering terms do not appear, although they are easily accommodated, since the only particulates occurring in the present application are the soot particles which are much too small to scatter significantly.

Equation (22) is solved within discretizations $\mathrm{d}\Omega$ of the whole solid angle Ω about selected directions. Assuming that $\tilde{E}$, k_g and k_s are constant over a finite distance increment δl, equation (22) may be integrated to yield the simple recurrence relation:

$$I_{n+1} = \frac{\tilde{E}}{\pi}\,(1 - \exp\,[-\,(k_g + k_s)\,\delta l]) + \\ + I_n \exp\,[-\,(k_g + k_s)\,\delta l] \tag{23}$$

where n and $(n + 1)$ are successive locations along the selected direction separated by the increment δl. The relation is applied along the chosen direction from known conditions at point, Q say (either guessed or pertaining to those of the previous iteration), on one wall to the point of impingement, P say, of the direction on a opposite wall.

If the hemisphere above point P is discretized into subangles $\mathrm{d}\Omega_r$, within which the intensity is considered to be uniform, the energy flux arriving at point P is:

$$q_{+,P} = \int_{\pi} I_P\,\Omega\,\mathrm{d}\Omega = \sum_r I_P \underset{r\to r}{\Omega}\,\mathrm{d}\Omega_r\,. \tag{24}$$

The wall boundary condition is:

$$q_{-,P} = (1 - \varepsilon_w)\,q_{+,P} + \varepsilon_w\,\tilde{E}_w \tag{25}$$

where $q_{-,P}$ is the energy leaving the wall at point P, ε_w is the wall emissivity, and $\tilde{E}_w = \sigma\,T_w^4$ is the wall emissive power. The value of $I_{o,r}$ at point Q, the initial value required for the application of the recurrence relation (23), is $q_{-,P} / \pi$. The net radiation heat flux is of course:

$$q_P = q_{+,P} - q_{-,P}\,. \tag{26}$$

The net heat gain or loss within a small control volume of the flow procedure is:

$$S_R = (I_{n+1} - I_n)\,\Omega\,\mathrm{d}\Omega\,\mathrm{d}A_w \tag{27}$$

where the locations n and $(n + 1)$ correspond to the "entry" and "exit" of the selected direction into and from a control volume, and A_w is the cell wall area projected normal to that direction. The energy sources S_R are appended to the energy-balance equation solved by the flow code.

The gas absorption coefficient k_g is calculated from the "two grey plus a clear gas" fit of [24]. Water vapour and carbon dioxide are the prime contributors to the gaseous radiation. The total gas emittance is expressed by:

$$\varepsilon_g = \sum_n a_{g,n}(T)\,[1 - \exp\,(k_{g,n}\,(p_{wv} + p_c)\,L] \tag{28}$$

where the summation n is over the three gases of the assumed mixture, the values of $k_{g,n}$ are presumed constant with the temperature dependence of the emittance being accommodated in the weighting coefficients $a_{g,n}$, p_{wv} and p_c are the partial pressures of water vapour and carbon dioxide, respectively, and L is the path length. The values of $k_{g,n}$ and $a_{g,n}$ are tabulated in [24]. The value of k_g required for these calculations is obtained from the pseudo grey approximation:

$$\varepsilon_g = 1 - \exp\,(-\,k_g\,L)$$

which has worked well in many furnace heat transfer computations.

3.7. Method of solution

The finite difference method used to solve the equations entails subdividing the furnace into a number of finite volumes or "cells". The solution algorithm was embodied in the TEACH programme

Table 1. Comparison between oil-fired and natural gas fired furnace performance

	natural gas	heavy oil
radiation to glass in W/m^2	$1.0661 \cdot 10^7$	$1.1194 \cdot 10^7$
convection to glass in W/m^2	$1.7979 \cdot 10^5$	$8.084 \cdot 10^4$
outlet temperature in K	1678	1650
maximum crown temperature in K	1830	1983
outlet velocity in m/s	16.1	15.8

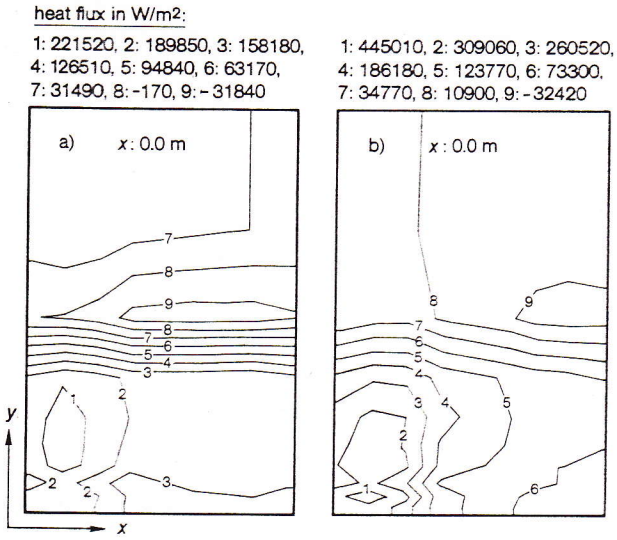

Figures 2a and b. Results of the calculated heat flux distribution to the glass at $x = 0$ m for a) a natural gas fired furnace, b) an oil-fired furnace.

for three-dimensional recirculating flows [25]. The convection terms were discretized by the hybrid central/upwind method [26]. The resultant difference equation has the form:

$$(a_P - S_P)\,\phi_P = \sum_n a_n\,\phi_n + S_0 \qquad (29)$$

where

$$a_P \equiv \sum a_n, \text{ and } \sum_n$$

denotes summation over the six neighbouring nodes; ϕ_P and ϕ_n mean the values of the variable ϕ for the point P and its neighbourhood points (D, E, N, S, U, W), respectively. One such equation exists for every scalar variable at every grid node. In the case of the velocities similar equations apply, but the control volumes are displaced such that they pass through the pressures driving the component in question, necessitating minor changes to the coefficient expressions.

The velocities and pressures are calculated by a variant of the SIMPLE algorithm [27]. As presented there, this algorithm involves the solution of the momentum equations using the prevailing pressures $\bar{p}^*$ to yield an intermediate velocity field denoted by $\bar{u}^*$; then velocity corrections are defined, linked to corresponding pressure corrections by relations of the form:

$$\bar{u}'_b = D^u_n\,(\bar{p}'_n - \bar{p}'_P) \qquad (30)$$

where $D^u_n \equiv \partial u_b / \partial(p_n - p_P)$ is evaluated from the relevant momentum equation and the subscript b denotes the control volume boundary location. Equation (30) is substituted into the integrated form of the continuity equation to give:

$$a_P\,\bar{p}' = \sum_n a_n\,\bar{p}' + S_0 \qquad (31)$$

from which p' and hence u' are determined. Equation (31) may be recognized as a form of Poisson's equation for the pressure correction, in which $S_0 \equiv -\sum_b \dot{m}_b$ is the local continuity imbalance of the momentum-based $\bar{u}^*$ velocities. Following the solution of this equation, the corrections are applied by setting $\bar{u} = \bar{u}^* + \bar{u}'$, $\bar{p} = \bar{p}^* + \bar{p}'$, and the entire procedure is repeated until momentum and continuity are both satisfied.

The calculations of the remaining dependent variables, as well as the updating of the thermodynamic and transport properties, are imbedded into the above sequence, but are not necessarily invoked at every cycle. For example, the radiation variables are recalculated less frequently than the others. The solution of the individual equations sets is obtained by a form of Gauss-Seidel line-by-line iteration.

4. Results

4.1. Some computational information

The present prediction procedure has been applied to the solution of the processes in a full-scale industrial glass furnace. The mildly arched crown was accommodated with small error within the orthogonal mathematical framework by: firstly, suitable adjustments to the area coefficients of the finite-difference equations, and secondly, the appending of extra terms to these equations to account for the extra mass fluxes entering a finite-difference cell consequent of the inclination of the cell wall with respect to the coordinate direction.

The row of individual gas burners was simulated by a slot. The real burner-inlet velocities and momenta were always maintained. Normally, the fuel jets were inclined upwards while the incoming air stream was usually directed slightly downwards. For the case of oil firing the spray is supposed to evaporate instantaneously in the grid cell adjacent to the plane of the atomizers. The presence of the spray was made known to the governing equations for the gas phase through appropriate source terms. This is a major simplification which is justified only when the near burner field is not of primary interest. A more

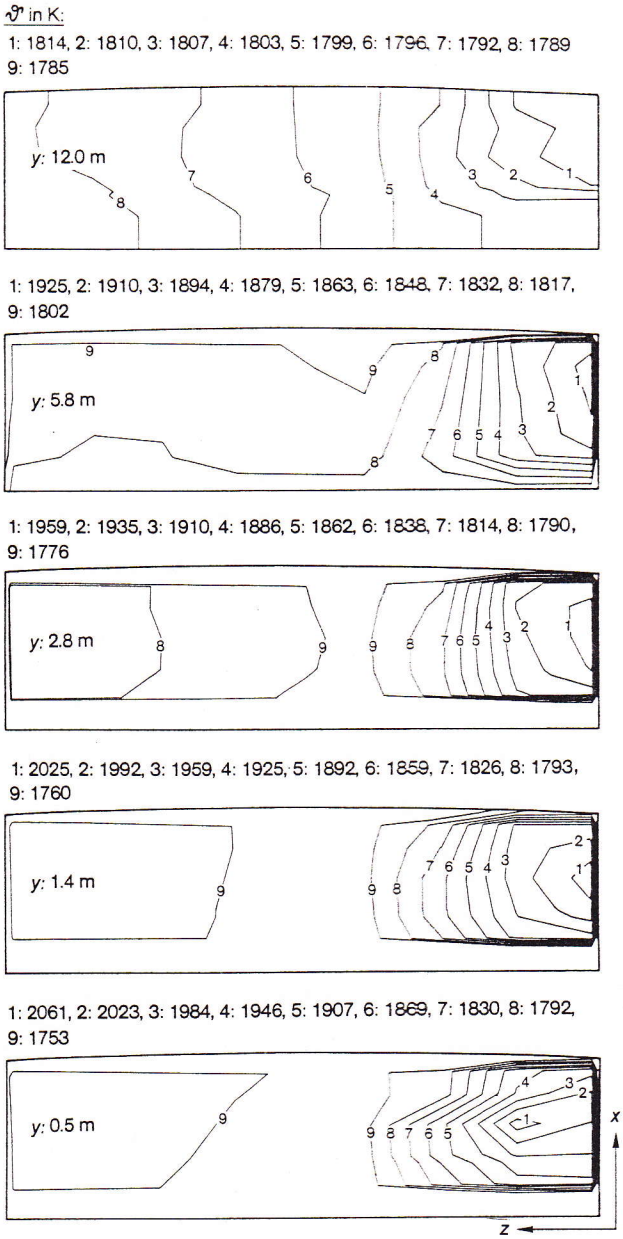

Figure 3. Results of the calculated temperature fields in the gas at different y values for a natural gas fired furnace.

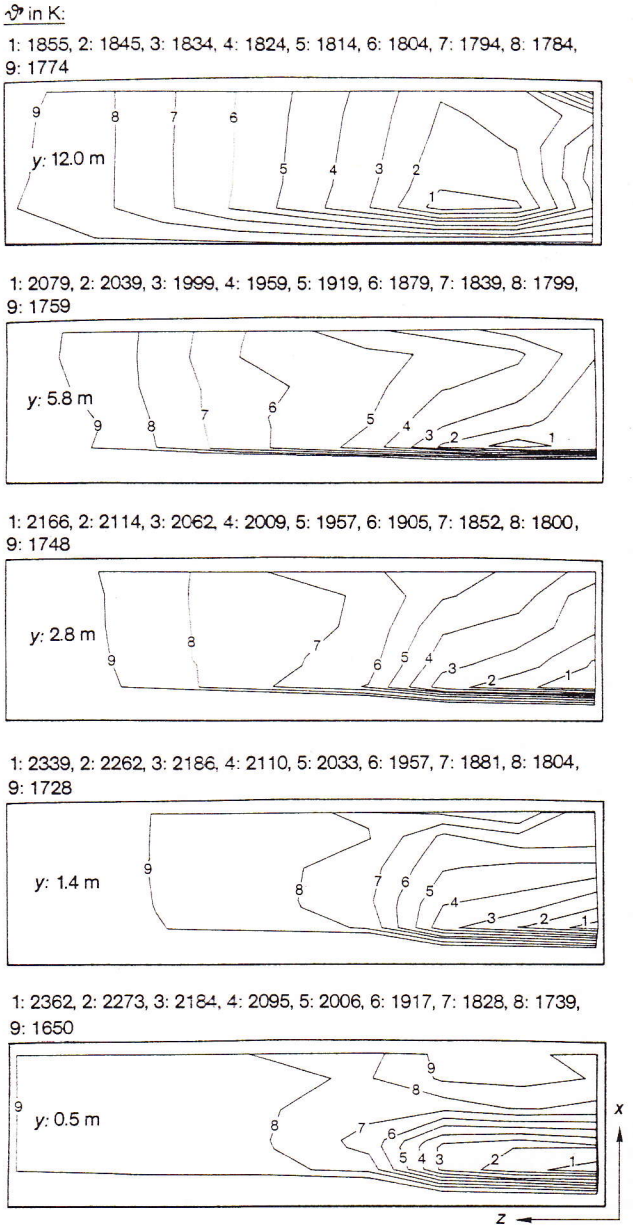

Figure 4. Results of the calculated temperature fields in the gas at different y values for an oil-fired furnace.

elaborate simulation would track droplet flights but the added computational expense could not be justified at this stage.

Boundary condition information has been stored two- rather than three-dimensionally for economy purposes. The finite-difference equations are solved by alternating direction line iteration in the $x-y$ planes. Because of the loosely parabolic nature of the flow, away from the entry port and towards the exit port, a considerable economic advantage accrued from the use of a plane-by-plane solution approach with the "sweeps" being conducted in the z direction. Because of the elliptic behaviour of pressure, it was found necessary to compute and store the coefficients of the pressure correction finite-difference equation three-dimensionally.

The performances of the furnace burning natural gas and heavy fuel oil for a firing rate of 30 MW and 8 % excess air in both cases have been compared.

4.2. Nature of radiation emission from natural gas and fuel oil flames

Flame emissivity is defined as the fraction of black-body radiation which is emitted by the flame. Hydrocarbon flames may emit "luminous" thermal radiation, caused by suspended solid soot particles as well as "non-luminous" radiation caused by changes in the vibrational and rotational energy levels of carbon dioxide, and water vapour and other gases whose molecular structure is asymmetric. Fuel oil, with much greater carbon/hydrogen ratio than the

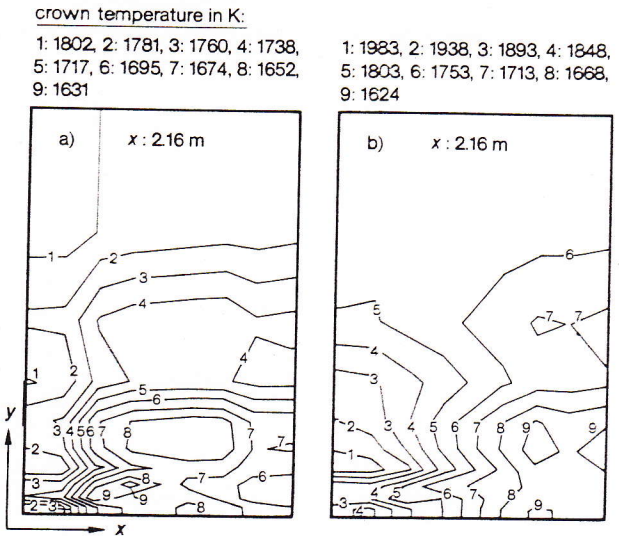

Figures 5a and b. Results of the calculated crown temperature distribution at $x = 2.16$ m for a) a natural gas fired furnace, b) an oil-fired furnace.

natural gas, burns with a strongly luminous flame. Natural gas, on the other hand, displays an interesting versatility: It can be burnt with a clean blue non-luminous flame, or with considerable luminosity, due to the cracking of the methane at about 1000 °C in the absence of oxygen. One method of promoting cracking is to design a baffle into the port bottom in order to delay the mixing of gas with combustion air [28]. This system is not popular because the resulting flame is not easily controlled.

A more effective self-carburization is achieved by passing 25 to 30 % of the natural gas through a helical coil which is exposed to the heat developed in the first portion of the main gas flame. This type of burner has proved its worth in a direct-fired metal sheet bar furnace [29] but its application to the high-temperature environment of a glass furnace port is probably not practical.

Due to different characteristics of the radiation emission from the two flames (oil and gas) the mechanisms of heat transfer to the glass in the two cases are different. In the case of the oil-firing furnace, most of the radiation to the crown is reradiated by the refractory and reabsorbed by the luminous flame. Thus, a much smaller proportion of the crown radiation penetrates the flame to reach the glass bath. It has been reported that in the case of oil, the energy transmitted by the flame is in order of 60 %, the rest being provided by the crown [30]. In the case of a furnace with a non-luminous gas flame, the crown plays a major part in transferring heat to the glass bath, because this type of flame is largely transparent to radiation. Most of the heat radiated from the flame will be absorbed by the crown and reradiated with only a relatively small amount being reflected. The absorbed energy is then reradiated over a much wider spectral band, as the crown converts the highly selective gas radiation into the normal continous emissions of a solid body. The reflected radiation, having the same wavelength as that originally emitted by the gas, is mainly reabsorbed by the gas.

Flame temperature is largely determined by furnace operating conditions and by the preheat of combustion air in the regenerators.

4.3. Discussion

Table 1 compares some key performance criteria for heavy oil and natural gas firing. The total radiative heat flux to the glass is 5 % higher for the case of the oil-firing furnace. Nevertheless, the distribution of the heat flux to the glass is less uniform in the case of oil (figures 2a and b). The radiative heat flux to the glass from the oil flame is as much as 100 % greater than for the case of natural gas flame in a very small area near the burner. This difference is reduced with increasing distance away from the burner towards the outlet because of the higher gas temperature of the natural-gas flame in the half of the furnace in front of the outlet. The convective heat transfer is higher in the case of natural gas, possibly due to the higher level of temperature of the gas in some parts of the furnace and to the higher fuel flow rates (another possible reason is the greater water-vapour content in the natural gas combustion products).

The gas temperature distribution for the oil-firing case is less uniform than in the case of natural gas (compare figures 3 and 4) with localised higher temperatures near the burner. This is due to the localised high soot content of the oil flame and because the "smoothing" effect of radiation is more for the more transparent gas flame. In the $y = 0.5$ m plane the maximum temperature is 200 K greater and the minimum is 100 K smaller for oil firing than for natural gas. This effect diminishes with the distance away from the burner plane. At the opposite wall ($y = 12.0$ m) the corresponding differences are only 40 and 8 K. The calculated temperatures for oil firing in the right hand side of the furnace are lower than in the natural gas case.

The maximum crown temperature is 180 K higher in the calculation for oil firing but this peak of temperature occurs only in a very small region near the burner (figures 5a and b). The distribution of temperature on the crown surface is less uniform in the fuel oil calculation for the same reason as for the heat flux distribution case. The minimum temperature is lower by 10 K in the case of oil. In general, the crown temperatures are higher in the oil-fired furnace due to higher radiation heat transfer from the flame.

The predicted contours of soot concentration are shown in figure 6. Soot production is essentially zero for mixture fractions less than that corresponding to the incipient sooting limit (figures 6 and 7). The

soot concentration in kg/m3:

1: $2 \cdot 10^{-7}$, 2: $1.7 \cdot 10^{-7}$, 3: $1.4 \cdot 10^{-7}$, 4: $1.2 \cdot 10^{-7}$, 5: $0.82 \cdot 10^{-7}$, 6: $0.66 \cdot 10^{-7}$, 7: $0.33 \cdot 10^{-7}$, 8: $0.13 \cdot 10^{-7}$

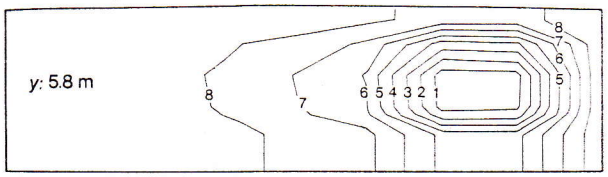

1: $2.6 \cdot 10^{-6}$, 2: $2.2 \cdot 10^{-6}$, 3: $1.9 \cdot 10^{-6}$, 4: $1.5 \cdot 10^{-6}$, 5: $1.2 \cdot 10^{-6}$, 1: $0.86 \cdot 10^{-6}$, 7: $0.51 \cdot 10^{-6}$, 8: $0.12 \cdot 10^{-6}$

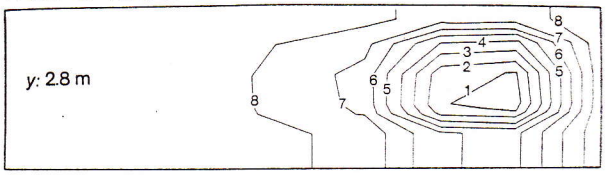

1: $1.2 \cdot 10^{-5}$, 2: $1.0 \cdot 10^{-5}$, 3: $0.88 \cdot 10^{-5}$, 4: $0.72 \cdot 10^{-5}$, 5: $0.66 \cdot 10^{-5}$, 6: $0.40 \cdot 10^{-5}$, 7: $0.24 \cdot 10^{-5}$, 8: $0.08 \cdot 10^{-5}$

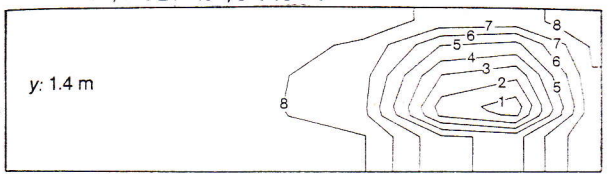

1: $3.2 \cdot 10^{-5}$, 2: $2.7 \cdot 10^{-5}$, 3: $2.3 \cdot 10^{-5}$, 4: $1.9 \cdot 10^{-5}$, 5: $1.6 \cdot 10^{-5}$, 6: $1.1 \cdot 10^{-5}$, 7: $0.69 \cdot 10^{-5}$, 8: $0.21 \cdot 10^{-5}$

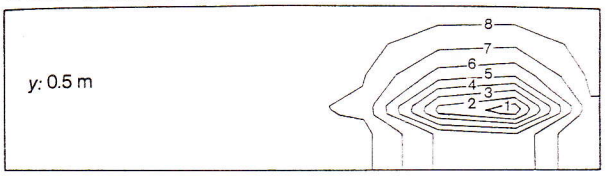

1: $1.1 \cdot 10^{-4}$, 2: $0.94 \cdot 10^{-4}$, 3: $0.79 \cdot 10^{-4}$, 4: $0.65 \cdot 10^{-4}$, 5: $0.60 \cdot 10^{-4}$, 6: $0.36 \cdot 10^{-4}$, 7: $0.22 \cdot 10^{-4}$, 8: $0.072 \cdot 10^{-4}$

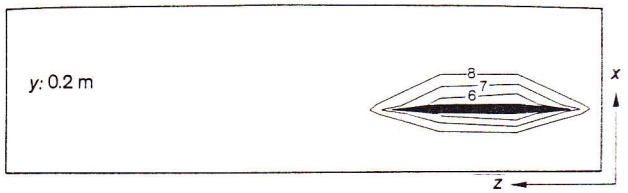

Figure 6. Predicted contours of soot concentrations at different y values for an oil-fired furnace.

mixture fraction:

1: 0.040, 2: 0.039, 3: 0.039, 4: 0.038, 5: 0.038, 6: 0.037, 7: 0.037, 8: 0.036

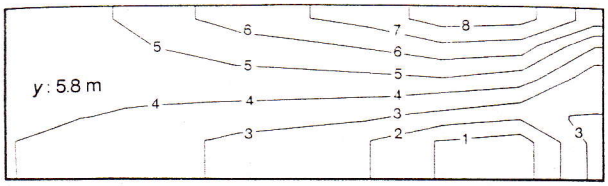

1: 0.043, 2: 0.041, 3: 0.040, 4: 0.038, 5: 0.037, 6: 0.036, 7: 0.034, 8: 0.033

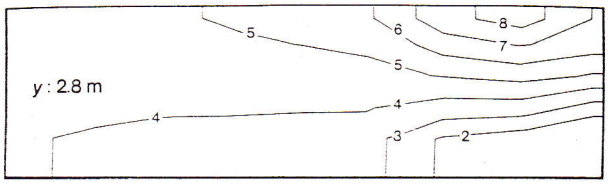

1: 0.045, 2: 0.042, 3: 0.040, 4: 0.037, 5: 0.036, 6: 0.032, 7: 0.029, 8: 0.027

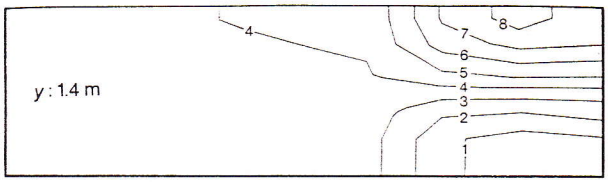

1: 0.054, 2: 0.049, 3: 0.043, 4: 0.038, 5: 0.033, 6: 0.027, 7: 0.022, 8: 0.017

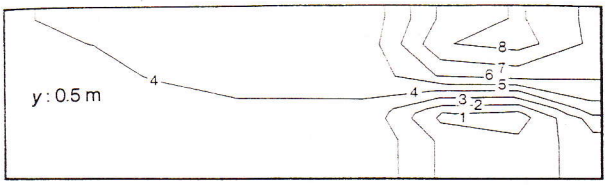

1: 0.11, 2: 0.099, 3: 0.084, 4: 0.069, 5: 0.054, 6: 0.039, 7: 0.024, 8: 0.0094

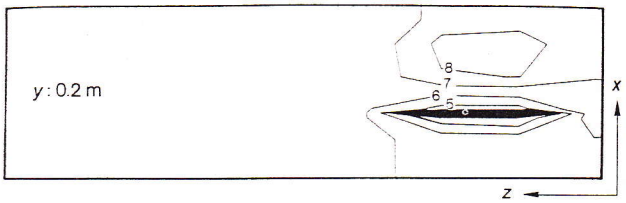

Figure 7. Predicted contours of mixture fraction at different y values for an oil-fired furnace.

maximum soot mass concentration ($1.1 \cdot 10^{-4}$ kg/m^3) occurs in the $y = 0.2$ m plane in the burner region. Thereafter the soot concentrations are rapidly diminished by oxidation and at the $y = 5.8$ m plane they are practically zero. Although there are no measured values of soot mass concentration in this particular furnace, these values agree with measurements in other furnaces (e.g. the experimental results obtained by Abbas [31]). The soot mass concentration is zero at the furnace outlet. A strong similarity can be observed between the contours of m_{fu} (figure 8) and the contours of m_s (figure 6). This reflects the strong influence of the amount of insufficiently mixed fuel in regions of high temperature.

The higher and less uniformly distributed temperatures, the presence of soot, SO_2 and V_2O_5 in the furnace atmosphere for the case of oil firing contribute to the faster ageing of these furnaces. Natural gas fired furnaces have longer lives. The reasons for this are mainly the negligible sulphur content of natural gas compared with up to 2 % in oil and the complete absence of vanadium in natural gas. Vanadium contributes V_2O_5 to the ash from oil flames, which is highly corrosive to refractories, particularly when accompanied by traces of Na_2O. Ash dropping into the glass is also undesirable because of the powerful colouring property of vanadium oxide. Sulphur contributes SO_2 to the furnace atmosphere, causing sodium sulphate deposits, which can also fall into the melt and cause problems of glass quality. Another important factor affecting the furnace life is the temperature of the

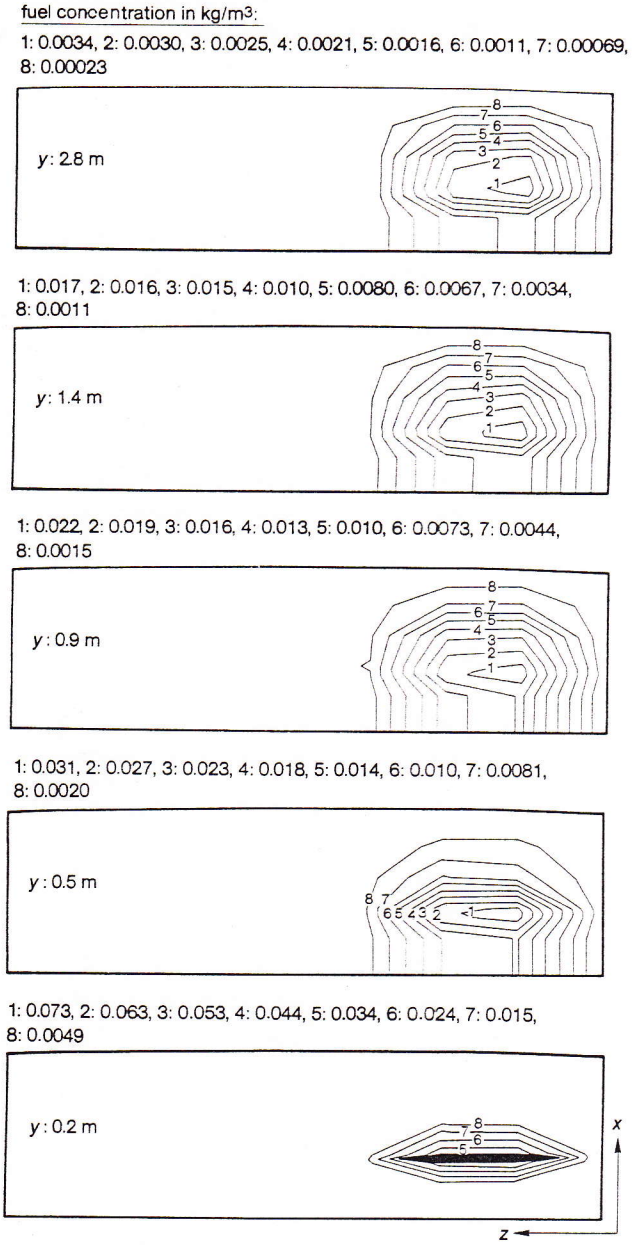

Figure 8. Predicted contours of fuel concentrations at different y values for an oil-fired furnace.

crown, which for a natural gas firing furnace is lower and more uniform.

On the whole the natural gas fired furnace is cleaner and less polluting than the oil-fired one. However, the present paper does not address the problem of NO_x emission. Natural gas fired furnaces produce high quantities of thermal NO_x. Future studies should focus on detailed comparison of NO_x formation for oil-fired furnaces and natural gas fired furnaces, respectively, and the influence of geometry and operating conditions on NO_x emission.

5. Concluding remarks

The paper has described the application of a very useful and general prediction procedure to a full-scale industrial glass furnace. The performances of the furnace firing natural gas and fuel oil have been compared.

The main difference between the performance of the two fuels (natural gas and heavy oil) is due to the greater emissivity of the oil flame and consequent greater heat transfer to the glass bath. In the present study the radiation from the oil flame is 5 % higher than that from the gas flame. The same excess air level (8 %) for both fuels has been assumed. In reality, it ought to be feasible to operate the gas-fired furnace at a slightly lower level which would decrease the heat-transfer discrepancy between the two fuels. Because the performance difference is small, natural gas flames are almost universally adopted as natural gas fired furnaces have longer lives, are cleaner and emit less pollutant than the oil-fired ones.

6. Nomenclature

6.1. Symbols

A_w	cell wall area
a_n	finite difference equation coefficient for the neighbour points (D, E, N, S, U, W) of P
a_P	finite difference equation coefficient for point P
C_{pj}	constant-pressure specific heat of species j in J/(kg K)
C_1, C_2	constants
E	activation energy in J/mol
$\bar{E}$	general black body emissive power
$\bar{E}_w$	black body emissive power of the wall
f	mixture fraction
g	variation of mixture fraction
g_i	gravitational acceleration in i direction in m/s^2
$\bar{h}$	mixture specific enthalpy
$\tilde{h}$	time mean stagnation enthalpy in J/kg
I	intensity of radiant energy in W/(m^2 sr)
k	kinetic energy in m^2/s^2
k_g, k_s	absorption coefficients of gas and soot, respectively, in m^{-1}
L	path length in m
l	distance in m
M_j	molecular weight of species j
$\bar{m}_j$	mass fraction of species j
$P(f)$	normal probability density function
P_{fu}	fuel production rate
P_l	chemical rate of production of species l
P_{s+}	soot production rate
P_{s-}	soot consumption rate
p	pressure in Pa
q_P	energy flux at point P on wall boundary in W/m^2
$\underline{R}$	universal gas constant in J/(mol K)
$\bar{S}$	source term defined by equation (4)
S_P, S_0	source terms of the finite-difference equations
S_φ	source term in φ equations
s_{fu}	fuel stoichiometric ratio
s_j	stoichiometric oxygen requirement of unit mass of species j
s_s	soot stoichiometric ratio
T	temperature in K
u_i	velocity component in i direction in m/s
x_i	Cartesian coordinate in m
Γ_h	fluid thermal conductivity divided by its constant-pressure specific heat
Γ_k	term in equations (10 and 11) defined via equation (8)
Γ_l	mass diffusion coefficient of species l
Γ_ε	term in equations (10 and 11) defined via equation (8)
Γ_φ	molecular exchange coefficient for a variable ϕ
$\Gamma_{\varphi,t}$	turbulent exchange coefficient for a variable ϕ

δ_{ij} Kronecker's delta
ε dissipation rate of turbulent energy in m^2/s^3
ε_g total gas emittance
ε_w emissivity of the wall
μ laminar viscosity in kg/(m s)
μ_t turbulent viscosity in kg/(m s)
ϱ density in kg/m^3
σ Stefan-Boltzmann constant of radiation
$\sigma_{\phi,t}$ Prandtl number for a variable ϕ
Φ equivalent ratio (equation (12))
ϕ surrogate variable f, g, $\bar{h}$, k, m_s, and ε, single passive scalar (equation (15))
Ω solid angle in sr

6.2. Superscripts

* guessed value
' fluctuation component
¯ time-averaged value

6.3. Subscripts

b control volume boundary location
c carbon dioxide
fu fuel
g gas
in inlet
l chemical species
n neighbouring nodes of point P
ox oxidant
P point P
s soot
t turbulent
w wall
wv water vapour

7. References

[1] Wu, H. L.: Comparison of the performance of natural gas and oil flames in a cylindrical furnace. J. Inst. Fuel **42** (1969) p. 316–322.

[2] Pai, B. R.; Bartelds, H.; Michelfelder, S.: An experimental investigation on the influence of operational and design variables on heat transfer to the furnace hearth. International Flame Research Foundation (IFRF), Ijmuiden. Doc. no. F 36/a/6. 1975.

[3] Della-Casa, H.; Marque, D.: Les travaux du G.E.F.G.N. conduisant à des économies d'énergie. Rev. Gén. Therm. **15** (1976) no. 169, p. 51–66.

[4] Datschefski, G.: Natural-gas firing in a cross-fired glass melting furnace. Glass Technol. **8** (1967) no. 6, p. 148–153.

[5] Buschmann, H.: Erdgas in der Glasindustrie. Glastech. Ber. **38** (1965) no. 3, p. 86–92.

[6] Lange, M. H. de: Einsatz des Erdgases in der Glasindustrie. Glastech. Ber. **40** (1967) no. 9, p. 337–340.

[7] Leveque, M.: Les combustibles liquides ou gazeux et la fusion du verre. Rev. Gén. Therm. **11** (1972) no. 130, p. 883–890.

[8] Abbott, E.: A comparison of glass furnace operation with oil and natural gas. Glass Technol. **18** (1977) no. 5, p. 143–147.

[9] Launder, B. E.; Spalding, D. B.: Mathematical models of turbulence. London: Acad. Press 1972.

[10] Hinze, J. O.: Turbulence. New York, Toronto, London: McGraw-Hill 1959.

[11] Gosman, A. D.; Lockwood, F. C.; Megahed, I. E. A. et al.: The prediction of the flow, reaction and heat transfer in the combustion chamber of a glass furnace. Presented at: AIAA 18th Aerospace Sciences Meeting, California, 1980.

[12] Pun, W. M.; Spalding, D. B.: A procedure for predicting the velocity and temperature distribution in a confined, steady turbulent, gaseous diffusion flame. In: Proc. Int. Astronautical Federation Meeting, Belgrade 1967.

[13] Lockwood, F. C.; Naguib, A. S.: The prediction of the fluctuations in the properties of free round jet, turbulent diffusion flames. Comb. Flame **24** (1975) p. 109–124.

[14] Spalding, D. B.: Concentration fluctations in a round turbulent free-jet. Chem. Eng. Sci. **26** (1971) no. 1, p. 95–107.

[15] Wagner, H. G. G.: Soot formation in combustion. In: 17th Symposium (International) on Combustion, Leeds (England) 1978. Pittsburgh, PA: The Combustion Institute 1978. p. 3–19.

[16] Khan, I. M.; Greeves, G.: A method for calculating the formation of soot in Diesel engines. In: Afgan, N. H.; Beer, J. M. (eds.): Heat transfer in flames. New York: Wiley 1974. p. 391–402.

[17] Abbas, A. S.; Koussa, S. S.; Lockwood, F. C.: The prediction of a variety of heavy oil flames. In: Proc. ASME, Winter Ann. Meet., Washington, 1981.

[18] Glassman, I.; Yaccarino, P.: The temperature effect in sooting diffusion flames. In: 18th Symposium (International) on Combustion, Waterloo (Canada) 1980. Pittsburgh, PA: The Combustion Institute 1980.

[19] Magnussen, B. F.; Hjertager, B. H.: On mathematical modelling of turbulent combustion with special emphasis on soot formation and combustion. In: 16th Symposium (International) on Combustion, Cambridge, MA, 1976. Pittsburgh, PA: The Combustion Institute 1976. p. 719–729.

[20] Tennekes, H.; Lumley, J. L.: A first course in turbulence. Cambridge, MA: MIT Press 1973.

[21] Lockwood, F. C.; Shah, N. G.: A new radiation solution method for incorporation in general combustion prediction procedures. In: 18th Symposium (International) on Combustion, Waterloo (Canada) 1980. Pittsburgh, PA: The Combustion Institute 1980. p. 1405–1414.

[22] Megahed, I. E. A.: The prediction of three-dimensional gas-fired combustion chamber flows. London Univ., Ph. D. thesis 1979.

[23] Carvalho, M. G.: Computer simulation of a glass flow furnace. London Univ., Ph. D. thesis 1983.

[24] Truelove, J. S.: A mixed grey gas model for flame radiation. AERE Harwell, report no. HL76/3448/KE. 1976.

[25] Gosman, A. D.; Humphrey, J. A. C.; Vlachos, N. S.: TEACH-3E: A general computer program for three-dimensional recirculating flows. Dept. of Mech. Eng., Imperial College, London, report no. CHT/76/10. 1976.

[26] Spalding, D. B.: A novel finite difference formulation for differential expressions involving both first and second derivatives. Int. J. Numer. Methods Eng. **4** (1972) p. 551–559.

[27] Patankar, S. V.; Spalding, D. B.: A calculation procedure for heat, mass and momentum transfer in three-dimensional parabolic flows. Int. J. Heat Mass Transfer **15** (1972) p. 1787–1806.

[28] Trinks, W.: Industrial furnaces. 3rd ed. Vol. 2. London, New York: Wiley 1955. p. 49.

[29] Demin, G. I.; Pluzhnikov, A. I.: Versuche mit keramischen Rekuperatoren an einem Stahlschmelzofen. (Orig. Russ.) Stal **21** (1961) no. 9, p. 853–856. (Engl. transl. in: Steel (1961) no. 9, p. 697–700.)

[30] Cabre, J. M.; Valle, F.: Situation actuelle de l'utilisation du gaz naturel dans les fours de fusion de verre. In: Symposium sur l'élaboration du verre (fusion et affinage), Madrid 1973. Charleroi: Union Scientifique Continentale du Verre 1974. p. 93–117.

[31] Abbas, A. S.: The prediction of the performance of heavy oil-fired combustors. London Univ., Ph. D. thesis 1982.

90R0967